Phase anomalies in Talbot light carpets of self-images

Myun-Sik Kim,[1,*] Toralf Scharf,[1] Christoph Menzel,[2] Carsten Rockstuhl,[2] and Hans Peter Herzig[1]

[1]*Optics & Photonics Technology Laboratory, Ecole Polytechnique Fédérale de Lausanne (EPFL), Neuchâtel,CH-2000, Switzerland*

[2]*Institute of Condensed Matter Theory and Solid State Optics, Abbe Center of Photonics, Friedrich-Schiller-Universität Jena, 07743 Jena, Germany*

**myunsik.kim@epfl.ch*

Abstract: An interesting feature of light fields is a phase anomaly, which occurs on the optical axis when light is converging as in a focal spot. Since in Talbot images the light is periodically confined in both transverse and axial directions, it remains an open question whether at all and to which extent the phase in the Talbot images sustains an analogous phase anomaly. Here, we investigate experimentally and theoretically the anomalous phase behavior of Talbot images that emerge from a 1D amplitude grating with a period only slightly larger than the illumination wavelength. Talbot light carpets are observed close to the grating. We concisely show that the phase in each of the Talbot images possesses an anomalous axial shift. We show that this phase shift is analogous to a Gouy phase of a converging wave and occurs due to the periodic light confinement caused by the interference of various diffraction orders. Longitudinal-differential interferometry is used to directly demonstrate the axial phase shifts by comparing Talbot images phase maps to a plane wave. Supporting simulations based on rigorous diffraction theory are used to explore the effect numerically. Numerical and experimental results are in excellent agreement. We discover that the phase anomaly, i.e., the difference of the phase of the field behind the grating to the phase of a referential plane wave, is an increasing function with respect to the propagation distance. We also observe within one Talbot length an irregular wavefront spacing that causes a deviation from the linear slope of the phase anomaly. We complement our work by providing an analytical model that explains these features of the axial phase shift.

OCIS codes: (050.1950) Diffraction gratings; (050.5080) Phase shift; (260.1960) Diffraction theory; (070.6760) Talbot and self-imaging effects; (180.3170) Interference microscopy.

References and links

1. F. Talbot, "Facts relating to optical science. No. IV," Philos. Mag. **9**, 401–407 (1836).
2. L. Rayleigh, "On copying diffraction gratings and some phenomena connected therewith," Philos. Mag. **11**(67), 196–205 (1881).
3. J. C. Bhattacharya, "Measurement of the refractive index using the Talbot effect and a moire technique," Appl. Opt. **28**(13), 2600–2604 (1989).
4. G. Spagnolo, D. Ambrosini, and D. Paoletti, "Displacement measurement using the Talbot effect with a Ronchi grating," J. Opt. Soc. A **4**(6), S376–S380 (2002).
5. J. R. Leger, M. L. Scott, and W. B. Veldkamp, "Coherent addition of AlGaAs lasers using microlenses and diffractive coupling," Appl. Phys. Lett. **52**(21), 1771–1773 (1988).
6. J. R. Leger, "Lateral mode control of an AlGaAs laser array in a Talbot cavity," Appl. Phys. Lett. **55**(4), 334–336 (1989).
7. L. Stuerzebecher, T. Harzendorf, U. Vogler, U. D. Zeitner, and R. Voelkel, "Advanced mask aligner lithography: fabrication of periodic patterns using pinhole array mask and Talbot effect," Opt. Express **18**(19), 19485–19494 (2010).
8. P. Maddaloni, M. Paturzo, P. Ferraro, P. Malara, P. De Natale, M. Gioffrè, G. Coppola, and M. Iodice, "Mid-infrared tunable two-dimensional Talbot array illuminator," Appl. Phys. Lett. **94**(12), 121105 (2009).

#179273 - $15.00 USD Received 5 Nov 2012; revised 21 Dec 2012; accepted 26 Dec 2012; published 11 Jan 2013

9. F. M. Huang, N. Zheludev, Y. Chen, and F. Javier Garcia de Abajo, "Focusing of light by a nanohole array," Appl. Phys. Lett. **90**(9), 091119 (2007).
10. O. Bryngdahl, "Image formation using self-imaging techniques," J. Opt. Soc. Am. **63**(4), 416–419 (1973).
11. E. Bonet, J. Ojeda-Castañeda, and A. Pons, "Imagesynthesis using the Laueffect," Opt. Commun. **81**(5), 285–290 (1991).
12. J. C. Barreiro, P. Andrés, J. Ojeda-Castañeda, and J. Lancis, "Multiple incoherent 2D optical correlator," Opt. Commun. **84**(5-6), 237–241 (1991).
13. R. F. Edgar, "The Fresnel diffraction images of periodic structures," J. Mod. Opt. **16**, 281–287 (1969).
14. J. T. Winthrop and C. R. Worthington, "Theory of Fresnel images. I. Plane periodic objects in monochromatic light," J. Opt. Soc. Am. **55**(4), 373–381 (1965).
15. A. Kołodziejczyk, "Realization of Fourier images without using a lens by sampling the optical object," J. Mod. Opt. **32**, 741–746 (1985).
16. Y.-S. Cheng and R.-C. Chang, "Theory of image formation using the Talbot effect," Appl. Opt. **33**(10), 1863–1874 (1994).
17. S. Teng, Y. Tan, and C. Cheng, "Quasi-Talbot effect of the high-density grating in near field," J. Opt. Soc. Am. A **25**(12), 2945–2951 (2008).
18. M. Berry and S. Klein, "Integer, fractional and fractal Talbot effects," J. Mod. Opt. **43**(10), 2139–2164 (1996).
19. E. Noponen and J. Turunen, "Electromagnetic theory of Talbot imaging," Opt. Commun. **98**(1-3), 132–140 (1993).
20. Y. Lu, C. Zhou, and H. Luo, "Talbot effect of a grating with different kinds of flaws," J. Opt. Soc. Am. A **22**(12), 2662–2667 (2005).
21. F. J. Torcal-Milla, L. M. Sanchez-Brea, and J. Vargas, "Effect of aberrations on the self-imaging phenomenon," J. Lightwave Technol. **29**(7), 1051–1057 (2011).
22. M. Berry, I. Marzoli, and W. Schleich, "Quantum carpets, carpets of light," Physics World June, 39–46 (2001).
23. X.-B. Song, H.-B. Wang, J. Xiong, K. Wang, X. Zhang, K.-H. Luo, and L.-A. Wu, "Experimental observation of quantum Talbot effects," Phys. Rev. Lett. **107**(3), 033902 (2011).
24. M. S. Chapman, C. R. Ekstrom, T. D. Hammond, J. Schmiedmayer, B. E. Tannian, S. Wehinger, and D. E. Pritchard, "Near-field imaging of atom diffraction gratings: The atomic Talbot effect," Phys. Rev. A **51**(1), R14–R17 (1995).
25. S. Nowak, Ch. Kurtsiefer, T. Pfau, and C. David, "High-order Talbot fringes for atomic matter waves," Opt. Lett. **22**(18), 1430–1432 (1997).
26. P. Cloetens, J. P. Guigay, C. De Martino, J. Baruchel, and M. Schlenker, "Fractional Talbot imaging of phase gratings with hard x rays," Opt. Lett. **22**(14), 1059–1061 (1997).
27. B. J. McMorran and A. D. Cronin, "An electron Talbot interferometer," New J. Phys. **11**(3), 033021 (2009).
28. M. R. Dennis, N. I. Zheludev, and F. J. García de Abajo, "The plasmon Talbot effect," Opt. Express **15**(15), 9692–9700 (2007).
29. S. Cherukulappurath, D. Heinis, J. Cesario, N. F. van Hulst, S. Enoch, and R. Quidant, "Local observation of plasmon focusingin Talbot carpets," Opt. Express **17**(26), 23772–23784 (2009).
30. M.-S. Kim, T. Scharf, C. Menzel, C. Rockstuhl, and H. P. Herzig, "Talbot images of wavelength-scale amplitude gratings," Opt. Express **20**(5), 4903–4920 (2012).
31. M.-S. Kim, T. Scharf, C. Etrich, C. Rockstuhl, and H. H. Peter, "Longitudinal-differential interferometry: Direct imaging of axial superluminal phase propagation," Opt. Lett. **37**(3), 305–307 (2012).
32. M.-S. Kim, T. Scharf, S. Mühlig, C. Rockstuhl, and H. P. Herzig, "Gouy phase anomaly in photonic nanojets," Appl. Phys. Lett. **98**(19), 191114 (2011).
33. L. G. Gouy, "Sur une propriété nouvelle des ondes lumineuses," C. R. Acad. Sci. Paris **110**, 1251–1253 (1890).
34. R. W. Boyd, "Intuitive explanation of the phase anomaly of focused light beams," J. Opt. Soc. Am. **70**(7), 877–880 (1980).
35. D. Subbarao, "Topological phase in Gaussian beam optics," Opt. Lett. **20**(21), 2162–2164 (1995).
36. R. Simon and N. Mukunda, "Bargmann invariant and the geometry of the Güoy effect," Phys. Rev. Lett. **70**(7), 880–883 (1993).
37. S. J. M. Habraken and G. Nienhuis, "Geometric phases in astigmatic optical modes of arbitrary order," J. Math. Phys. **51**(8), 082702 (2010).
38. G. F. Brand, "A new millimeter wave geometric phase demonstration," Int. J. Infrared Millim. Waves **21**(4), 505–518 (2000).
39. P. Hariharan and P. A. Robinson, "The Gouy phase shift as a geometrical quantum effect," J. Mod. Opt. **43**, 219–221 (1996).
40. S. Feng and H. G. Winful, "Physical origin of the Gouy phase shift," Opt. Lett. **26**(8), 485–487 (2001).
41. I. G. Da Pazl, P. L. Saldanha, M. C. Nemes, and J. G. Peixoto de Faria, "Experimental proposal for measuring the Gouy phase of matter waves," New J. Phys. **13**, 125005 (2011).
42. T. D. Visser and E. Wolf, "The origin of the Gouy phase anomaly and its generalization to astigmatic wavefields," Opt. Commun. **283**(18), 3371–3375 (2010).
43. J. P. Rolland, K. P. Thompson, K.-S. Lee, J. Tamkin, Jr., T. Schmid, and E. Wolf, "Observation of the Gouy phase anomaly in astigmatic beams," Appl. Opt. **51**(15), 2902–2908 (2012).
44. A. E. Siegman, *Lasers* (University Science Books, Stanford, 1986).
45. M. Born and E. Wolf, *Principles of Optics*, 7th ed. (Cambridge University Press, Cambridge, 1999).
46. F. Gittes and C. F. Schmidt, "Interference model for back-focal-plane displacement detection in optical tweezers," Opt. Lett. **23**(1), 7–9 (1998).

#179273 - $15.00 USD Received 5 Nov 2012; revised 21 Dec 2012; accepted 26 Dec 2012; published 11 Jan 2013

47. B. Roy, S. B. Pal, A. Haldar, R. K. Gupta, N. Ghosh, and A. Banerjee, "Probing the dynamics of an optically trapped particle by phase sensitive back focal plane interferometry," Opt. Express **20**(8), 8317–8328 (2012).
48. L. Friedrich and A. Rohrbach, "Tuning the detection sensitivity: a model for axial backfocal plane interferometric tracking," Opt. Lett. **37**(11), 2109–2111 (2012).
49. R. W. Boyd, *Nonlinear Optics* 2nd ed. (Academic Press, San Diego, 1992).
50. S. Carrasco, B. E. A. Saleh, M. C. Teich, and J. T. Fourkas, "Second- and third-harmonic generation with vector Gaussian beams," J. Opt. Soc. Am. B **23**(10), 2134–2141 (2006).
51. C. Zhang, Y.-Q. Qin, and Y.-Y. Zhu, "Perfect quasi-phase matching for the third-harmonic generation using focused Gaussian beams," Opt. Lett. **33**(7), 720–722 (2008).
52. N. C. R. Holme, B. C. Daly, M. T. Myaing, and T. B. Norris, "Gouy phase shift of single-cycle picosecond acoustic pulses," Appl. Phys. Lett. **83**(2), 392–394 (2003).
53. C. R. Carpenter, "Gouy phase advance with microwaves," Am. J. Phys. **27**, 98–100 (1959).
54. J. F. Federici, R. L. Wample, D. Rodriguez, and S. Mukherjee, "Application of terahertz Gouy phase shift from curved surfaces for estimation of crop yield," Appl. Opt. **48**(7), 1382–1388 (2009).
55. A. B. Ruffin, J. V. Rudd, J. F. Whitaker, S. Feng, and H. G. Winful, "Direct observation of the Gouy phase shift with single-cycle terahertz pulse," Phys. Rev. Lett. **83**(17), 3410–3413 (1999).
56. H. He and X.-C. Zhang, "Analysis of Gouy phase shift for optimizing terahertz air-biased-coherent-detection," Appl. Phys. Lett. **100**(6), 061105 (2012).
57. B. E. A. Saleh and M. C. Teich, *Fundamentals of Photonics* (John Wiley & Sons, Inc., 1991).
58. H. Kogelnik and T. Li, "Laser Beams and Resonators," Appl. Opt. **5**(10), 1550–1567 (1966).
59. T. Ackemann, W. Grosse-Nobis, and G. L. Lippi, "The Gouy phase shift, the average phase lag of Fourier components of Hermite-Gaussian modes and their application to resonance conditions in optical cavities," Opt. Commun. **189**(1-3), 5–14 (2001).
60. J. Courtial, "Self-imaging beams and the Guoy effect," Opt. Commun. **151**(1-3), 1–4 (1998).
61. J. Hamazaki, Y. Mineta, K. Oka, and R. Morita, "Direct observation of Gouy phase shift in a propagating optical vortex," Opt. Express **14**(18), 8382–8392 (2006).
62. H. X. Cui, X. L. Wang, B. Gu, Y. N. Li, J. Chen, and H. T. Wang, "Angular diffraction of an optical vortex induced by the Gouy phase," J. Opt. **14**(5), 055707 (2012).
63. H. Chen, Q. Zhan, Y. Zhang, and Y.-P. Li, "The Gouy phase shift of the highly focused radially polarized beam," Phys. Lett. A **371**(3), 259–261 (2007).
64. X. Pang, G. Gbur, and T. D. Visser, "The Gouy phase of Airy beams," Opt. Lett. **36**(13), 2492–2494 (2011).
65. R. Gadonas, V. Jarutis, R. Paškauskas, V. Smilgevičius, A. Stabinis, and V. Vaičaitis, "Self-action of Bessel beam in nonlinear medium," Opt. Commun. **196**(1-6), 309–316 (2001).
66. P. Martelli, M. Tacca, A. Gatto, G. Moneta, and M. Martinelli, "Gouy phase shift in nondiffracting Bessel beams," Opt. Express **18**(7), 7108–7120 (2010).
67. W. Zhu, A. Agrawal, and A. Nahata, "Direct measurement of the Gouy phase shift for surface plasmon-polaritons," Opt. Express **15**(16), 9995–10001 (2007).
68. D. Chauvat, O. Emile, M. Brunel, and A. Le Floch, "Direct measurement of the central fringe velocity in Young-type experiments," Phys. Lett. A **295**(2-3), 78–80 (2002).
69. M. Vasnetsov, V. Pas'ko, A. Khoroshun, V. Slyusar, and M. Soskin, "Observation of superluminal wave-front propagation at the shadow area behind an opaque disk," Opt. Lett. **32**(13), 1830–1832 (2007).
70. L. Li, "New formulation of the Fourier modal method for crossed surface-relief gratings," J. Opt. Soc. Am. A **14**(10), 2758–2767 (1997).
71. M.-S. Kim, T. Scharf, S. Mühlig, C. Rockstuhl, and H. P. Herzig, "Engineering photonic nanojets," Opt. Express **19**(11), 10206–10220 (2011).
72. M.-S. Kim, T. Scharf, and H. P. Herzig, "Small-size microlens characterization by Multiwavelength High-Resolution Interference Microscopy," Opt. Express **18**(14), 14319–14329 (2010).
73. E. Lau, "Beugungserscheinungen an Doppelrastern," Ann. Phys. **437**(7-8), 417–423 (1948).
74. A. W. Lohmann and A. S. Marathay, "About periodicities in 3-D wavefields," Appl. Opt. **28**(20), 4419–4423 (1989).
75. A. W. Lohmann and J. Ojeda-Castaneda, "Spatial periodicities in partially coherent fields," Opt. Acta: Int. J. Opt. **30**(4), 475–479 (1983).
76. M. Thiel, M. Hermatschweiler, M. Wegener, and G. von Freymann, "Thin-film polarizer based on a one-dimensional–three-dimensional–one-dimensional photonic crystal heterostructure," Appl. Phys. Lett. **91**(12), 123515 (2007).
77. X. Pang, D. G. Fischer, and T. D. Visser, "Generalized Gouy phase for focused partially coherent light and its implications for interferometry," J. Opt. Soc. Am. A **29**(6), 989–993 (2012).
78. Q. Zhan, "Second-order tilted wave interpretation of the Gouy phase shift under high numerical aperture uniform illumination," Opt. Commun. **242**(4-6), 351–360 (2004).
79. J. T. Foley and E. Wolf, "Wave-front spacing in the focal region of high-numerical-aperture systems," Opt. Lett. **30**(11), 1312–1314 (2005).
80. T. D. Visser and J. T. Foley, "On the wavefront spacing of focused, radially polarized beams," J. Opt. Soc. Am. A **22**(11), 2527–2531 (2005).

#179273 - $15.00 USD Received 5 Nov 2012; revised 21 Dec 2012; accepted 26 Dec 2012; published 11 Jan 2013

1. Introduction

Diffraction and interference phenomena are manifestations of the wave nature of light. A prime example for such effect constitutes a grating that diffracts monochromatic incident light into discrete directions. Especially in the Fresnel diffraction regime, i.e., the region close to the surface of the grating, each diffraction order propagates at a certain angle and superposes with others in space. Such a superposition leads to interference and self-images of the grating can be observed. This self-imaging phenomenon was first discovered by Talbot in 1836 [1] and afterward called the Talbot effect. It connotes that the light field emerging from the grating possesses a periodicity in propagation direction, in addition to the periodicity in lateral directions imposed by the periodicity of the object. Such particular field distributions repeat at regular distances away from the grating surface. An analytic description for this distance was derived by Lord Rayleigh in 1881 and he called it the Talbot length [2].

These self-imaging effects play an important role in numerous applications. Examples are for the measurements of the refractive index [3], for sensing a distance or a displacement [4], for laser resonators [5, 6], lithography [7], array illumination [8], sub-wavelength focusing [9], imaging [10], lensless image synthesis [11] and 2D optical correlator [12]. Such appealing applications draw attention and led to intensive investigations; both experimentally and theoretically. The theoretical studies often focused on a discussion of the origin of the Talbot effect and associated phenomena while relying on different approximations. Work has been done in the framework of Fresnel diffraction [13], Fresnel images [14], Fourier images [15], and the theory of image formation [16]. Associated effects such as the quasi-Talbot effect [17] or the fractional and fractal Talbot effects [18] were equally investigated. Also, rigorous studies were done using, e.g., electromagnetic theory [19], the finite-difference time-domain (FDTD) method [20] and the Rayleigh-Sommerfeld formula to understand the impact of aberrations on the self-imaging process [21]. In physical optics, researchers discussed such effects down to the quantum mechanical level, i.e., the quantum Talbot effect [22, 23]. Such self-imaging phenomena are also not limited to optical waves. For instance, the Talbot effect exits for atomic matter waves [24, 25], x-ray [26], electron beams [27], and surface plasmons [28, 29].

Compared to the theoretical works, there are only few experimental investigations reported. In most of these experiments, the Talbot effect has been studied using gratings with periods much larger when compared to the wavelength, for example, in Refs. [20], [21] and [23]. This suggests a certain simplicity for the experiments since it is not difficult to accommodate the associated macroscopic scales. Moreover, and even surprisingly, the phase features are often not taken into account in these studies. Recently, a detailed experimental and theoretical study of the Talbot effect has been using a 1D amplitude grating with a period only slightly larger than the wavelength. There, detailed information of both amplitude and phase fields were provided [30]. The contributions of each diffraction order to the Talbot effect and the formation of self-images has been discussed. However, it can be expected that such fields may be characterized by much more interesting features. A prime example phase fields might feature, in general, is the anomalous axial phase shift [31]. In this work, we focus on the phase of light fields emerging from the grating surface that form Talbot images. Especially, the axial phase behavior of the light is of interest.

In the context of the Talbot effect, the occurrence of axial phase anomalies has never been observed nor discussed. Such phase anomalies, however, constitute a generic feature in phase fields that occur when light is converging as in a focal spot or is confined as in a photonic nanojet [32]. A Talbot carpet shows a light distribution that corresponds to an array of focal spots with a periodicity along both lateral and axial directions. By considering this to be the periodic analog of an isolated focal spot, phase anomalies are expected to occur in each self-imaging plane. Anomalous axial phase behavior of the wave fields has been drawing attention since Gouy's discovery in 1890 [33], which is called Gouy phase or phase anomaly. In general, the anomaly is characterized by an $\alpha \cdot \pi/2$ axial phase shift for a converging light wave passing through its focus upon propagating from $-\infty$ to $+\infty$. The factor α is a dimension-

#179273 - $15.00 USD Received 5 Nov 2012; revised 21 Dec 2012; accepted 26 Dec 2012; published 11 Jan 2013

related value, which equals 1 for a line focus representing the 2D case (i.e., a cylindrical wave) and equals 2 for a point focus representing 3D case (i.e., a spherical wave). Although, Gouy's discovery took place more than a hundred years ago, curiosity about the origin and physical meanings of this peculiar phenomenon continually stimulated discussions based on different theoretical perspectives. For example, the geometric properties of Gaussian beams [34], Berry's geometrical phase [35–38], and even quantum mechanics [39–41] have been considered to give insights into this effect. Recently, it has been also explored in the context of deviating wavefields, i.e., astigmatic wavefields [42, 43]. The importance of such anomalous phase features can be found in various physical problems, for instance, they contribute defining the resonance frequencies of laser cavities [44, 45], they can be used for optical trapping [46–48], and for higher harmonic generations [49–51]. Such phase anomalies are a general wave phenomenon and were found not just in optical waves, but also in acoustic waves [52], microwaves [38, 53], and terahertz waves [54–56]. In optical waves, various classes of beams exhibit the Gouy phase. Examples are general higher Gaussian modes like Hermite-Gaussian and Laguerre-Gaussian beams [44, 57–60], more specifically a vortex beam [61, 62], a radially polarized beam [63], the Airy beam [64], and the Bessel beam [65, 66]. In addition to such optical beams, surface plasmon-polaritons [67], matter waves [41], scattered hotspots (i.e., a photonic nanojet) [32], and diffracted hotspots (i.e., the spot of Arago) [68, 69] also show axial phase shifts. The amount of such axial phase shifts differs depending on the type of beams and the confinement situations. If one considers the analogy of multiple focal spots to the confined light in each self-imaging plane, the phase field in the Talbot images might naturally possess a phase anomaly too. Here, we will verify this hypothesis and determine the amount of the shift. A demonstration of the presence of the phase anomaly and the amount of the axial phase shift are the main subject of this work.

The Talbot images we use are generated by a wavelength-scale amplitude grating in the visible spectrum, which allows only three propagating diffraction orders (i.e., the 0th and ± 1st orders) that prevent a production of fractional or fractal Talbot images [18] and generate only self-images. To be precise, the amplitude grating we rely on has a period of $\Lambda = 1$ μm and the illumination wavelength is $\lambda = 642$ nm. The usage of such a high spatial frequency grating allows the experimental demonstration of the high-resolution light field measurement for the self-Talbot images. For experiments, we use a high-resolution interference microscope (HRIM) that facilitates the longitudinal-differential interferometry technique. The HRIM directly records the axial phase shift by comparing the measured phase with that of a reference plane wave *in situ* [31]. Therefore, it allows to measure directly the magnitude of the phase anomaly that is defined as the difference in phase of a given field to that of a referential plane wave. In order to verify the experimental results, rigorous simulations using Fourier Modal Method (FMM) are performed [70]. We rely here on a super-cell simulation that allows to take into account all the details of the finite sample. To understand the origin of such phase shifts in Talbot images, an analytical equation for the phase anomaly will be derived. We also briefly discuss about other phase features like the phase singularity that appears only in the self-imaging plane due to the destructive interference of the lowest three diffraction orders. This can find an application to measure the Talbot length with super-resolution.

2. Experiment and simulation

For the measurements of amplitude and phase in the entire 3D space, a high-resolution interference microscope (HRIM) is considered. Details of the experimental setup are reported elsewhere [71, 72]. A particular measurement mode of the HRIM allows longitudinal-differential (LD) interferometry [31] that directly measures the axial phase shift by comparing the phase of the object field with that of a reference plane wave *in situ*. In this study, all experimental and theoretical investigations were performed at a single wavelength of 642 nm (CrystaLaser: DL640-050-3). In passing we note that the laser source provides perfect coherent light and the light delivering system is based on a collimation using a spatial filtering technique that also assures perfect spatial coherence. The Talbot effect occurs in the

#179273 - $15.00 USD Received 5 Nov 2012; revised 21 Dec 2012; accepted 26 Dec 2012; published 11 Jan 2013

amplitude of the wave field only if it is perfectly coherent, as it holds for the present setup. However, even for incoherent light a longitudinal periodicity can be observed that was first described by Lau [73] and it also holds for partially coherent beams [74, 75].

The achievable spatial resolution for the amplitude fields is subject to the diffraction limit of the observing objective (in this case, a 100X/NA0.9 HC PL FLUOTAR from Leica Microsystems). LD interferometry requires an *in situ* reference plane wave. This provides direct information on the phase evolution of the referential plane wave. To include the referential plane wave in the object space, we design an integrated sample system that includes a wide opening. This opening is distant from the edge of the grating and serves as the passage of the unperturbed illumination, which provides the referential phase. The geometry of the integrated sample system is illustrated in Fig. 1. It has three distinct regions: An opening for the reference wave, an amplitude stop for spatial separation, and the grating region. The reference field is a 40-μm opening that is located next to a 30-μm opaque region to separate the grating and reference region. The grating is a 1D amplitude grating that has a period of 1 μm and a duty cycle of 0.5. The grating structures and the opaque region are made of 80-nm thick chromium (Cr) coating, which is opaque at the wavelength of interest and a metal coating that used for conventional mask structure of photolithography formed on a 1.5-mm-thick glass substrate (Compugraphics Jena GmbH). Illumination is in TM polarization with respect to the grating.

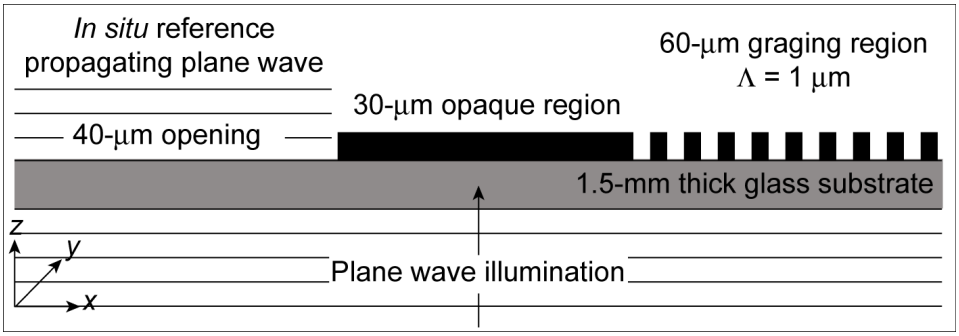

Fig. 1. Schematic geometry of the grating structure: the 1D amplitude grating of the period Λ = 1 μm and the duty cycle = 0.5, the 30-μm-wide opaque region, and the 40-μm-wide opening region where the *in situ* reference plane wave passes. Structures are fabricated on a 1.5-mm-thick glass substrate.

Eventually, what we want to probe in our experiments is the phase anomaly in a wave field that consists of three interfering plane waves, in our case, three propagating diffraction orders, that could have been also generated in the field upon interference of a finite number of plane waves. However, such scheme does not allow for the measurement of LD phase map in an unambiguous manner since an isolated plane wave that provides the referential phase advance cannot be incorporated into such measurement scheme. The beauty of the proposed sample structure shown in Fig. 1 is the integration of all the necessary structures into a single sample that can be equally measured at once. This is a clear advantage of devices that are discussed in the field of micro- and nano-optics, respectively. The integration of multiple functionalities into one sample is often very beneficial [76]. With this particularly designed sample, we can additionally demonstrate and study the presence of the boundary diffraction wave at the edge of the opaque region and, moreover, the propagation of an isolated diffraction order that is not superposed to other diffraction orders. These features can be observed at the edges of the opaque region. To be precise, at the left edge of the 30-μm opaque region in Fig. 1, a boundary diffraction wave emerges toward both the shadow (to the right) and opening (to the left) regions. At the right boundary of the opaque region, an isolated diffraction order emerges to the left into the shadow region and does not superpose with other orders of the grating. The diffraction orders emerging from the middle of the grating region superpose each other and eventually produce the Talbot images.

#179273 - $15.00 USD Received 5 Nov 2012; revised 21 Dec 2012; accepted 26 Dec 2012; published 11 Jan 2013

For the rigorous numerical calculation of the field distribution behind the grating the Fourier Modal Method is used [70]. It solves directly Maxwell's equations and only assumes the structure to be periodically arranged. Therefore, the finite structure is simulated within a super-cell approach, i.e., with an artificial super-period of P = 130 μm. It was verified that the size of the super-cell does not affect the conclusions to be drawn, i.e., it is large enough to consider the regions of interest as being isolated. The grating consists of 60 periods with the same period, filling fraction, and height as in the experiment. Left to the grating the opaque region with a width of 30 μm is considered. Further to the left, the opening with a width of 40 μm exists. Taking all together the super-cell has a period of 130 μm. The metal is assumed to be characterized by a refractive index of $n = 2.039 + i2.879$, corresponding to the index of chrome at a wavelength of 642 nm. The entire structure is placed on a substrate with index $n = 1.5$ and illuminated from the substrate with a TM polarized plane wave. Due to the large super-period, an excessive number of Fourier orders had to be taken into account ($N = 4001$) for the simulation in order to achieve convergent results. All intensity and phase distributions in the manuscript are shown such that $z = 0$ μm correspond to the terminating edge of the grating.

3. Intensity distributions: Talbot images and Talbot length

The simplest demonstration of the self-imaging effect is an intensity measurement that prominently shows the periodic intensity distributions corresponding to the grating period and an axial periodicity at repeated distances away from the grating surface. Figure 2 shows the measured and simulated *x*-*z* intensity distributions when the 1D grating structure from Fig. 1 is illuminated by a plane wave of 642 nm wavelength.

The region of interest (ROI) is the central 60-μm part, which covers a part of the opening and the grating and the full 30-μm opaque region. On the left hand side, the *in situ* reference plane wave with minimal perturbations passes through the opening. No light passes through the opaque region, $x = 5$ - 35 μm in Fig. 2. Only diffracted light emerges at certain angles from both edges of the opaque region. On the right hand side, $x = 35$ - 60 μm, the self-images of the grating appear, i.e., the Talbot images. Here, one can see a consequence of the finite grating. The diffraction angle of the ± 1st orders defines a geometrical region with an inclined edge where the three diffraction orders superpose and interfere to form the Talbot image. The inclination angle perfectly corresponds to the diffraction angle of the 1st order. For a period of $\Lambda = 1$ μm and a wavelength of $\lambda = 642$ nm, the 1st order diffraction order propagates at an angle of 39.9°. The region $x = 50$ - 60 μm shows Talbot images extending up to $z = 20$ μm. It corresponds to the upper limit of the region of interest. The simulation in Fig. 2(b) shows an excellent agreement with the measurement from Fig. 2(a).

While the boundary diffraction wave at the left edge of the opaque region is not prominently visible in both figures due to very low field strength, the single diffraction order emerging from the boundary between the opaque region and the grating is well resolved. This single diffraction order emerging toward the left from the grating, which is defined as the −1st order in our convention, demonstrates a tilting angle that corresponds to the diffraction angle of 39.9°. This is the vertical reflection of the inclination angle of the Talbot image zone in Fig. 2 that is defined by the + 1st order. Since in the present configuration only three diffraction orders propagate, i.e., the 0th and ± 1st, only self-Talbot images are found. This implies that there are neither quasi-Talbot images nor fractional Talbot images [17, 18] that are associated with higher diffraction orders. Each self-image plane has a lateral shift of half grating period. The distance between adjacent self-image planes is equal to half the Talbot length. In some literatures [e.g., Ref. [22]] this half-length is used as the Talbot length Z_T, but we adopt the original definition proposed by Lord Rayleigh [2], which is derived as

$$Z_T = \frac{\lambda}{1-\sqrt{1-\left(\frac{\lambda}{\Lambda}\right)^2}}. \qquad (1)$$

#179273 - $15.00 USD Received 5 Nov 2012; revised 21 Dec 2012; accepted 26 Dec 2012; published 11 Jan 2013

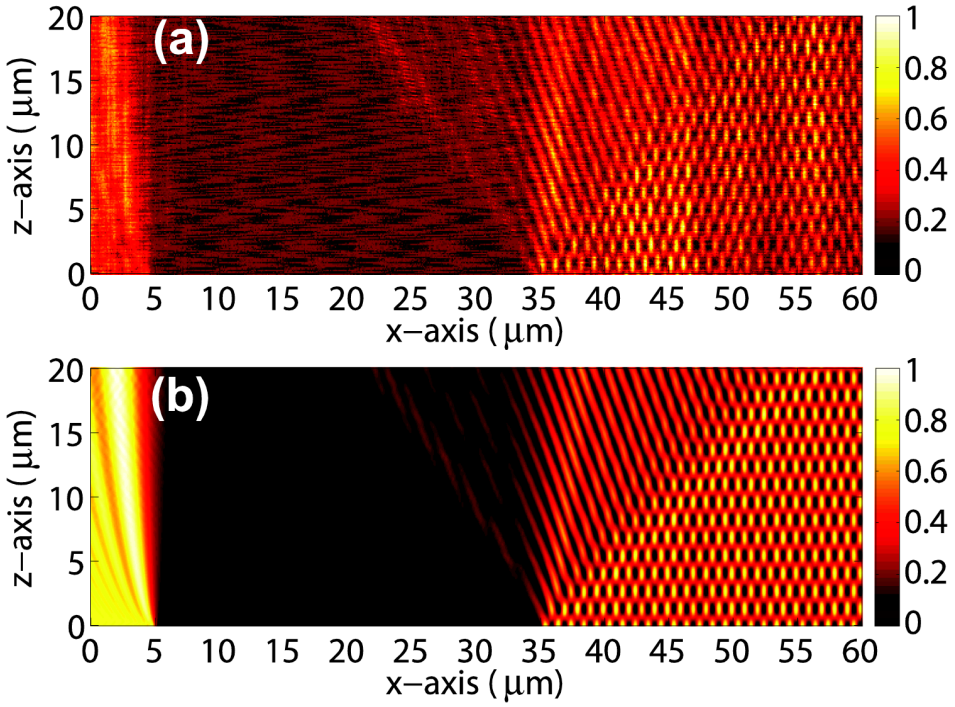

Fig. 2. The *x*-*z* intensity distribution emerging from the grating structure shown in Fig. 1. A plane wave is used for the illumination. (a) Measured and (b) simulated intensity distribution. The region of interest is the central 60-µm part of Fig. 1. Intensities are normalized.

He also suggested an approximation to Eq. (1) when the wavelengths λ is considered to be small compared to the period Λ of the structure. In this paraxial approximation the Talbot length can be expressed as

$$Z_{\mathrm{T}} = \frac{2\Lambda^2}{\lambda}. \qquad (2)$$

Our study is a prime example to demonstrate the invalidity of Eq. (2) when the period Λ tends to be in the order of the wavelength λ. Figure 3 shows the calculated Talbot length with respect to the grating period by using both Eqs. (1) and (2). The difference between results of two equations becomes prominent when Λ equals 5λ, where 1% difference occurs. Here, the difference in percentage is derived by comparing the difference with the actual Talbot length from Eq. (1). Analytically, the difference can reach 100% when the Talbot lengths equals the observation wavelength, hence Λ = λ. Already for the case of Λ = 1.56λ (i.e., Λ = 1 µm at λ = 642 nm), the difference is significantly increased up to almost 12%. Therefore, for our case, we can assert that Eq. (2) is not valid anymore and should not be used. Equation (1) is the exact analytical solution to verify the experimental and numerical results. Figures 2(a) and 2(b) both demonstrate the Talbot length Z_T = 2.8 µm that perfectly matches with the result of Eq. (1) while Eq. (2) would lead to Z_T = 3.1 µm.

#179273 - $15.00 USD Received 5 Nov 2012; revised 21 Dec 2012; accepted 26 Dec 2012; published 11 Jan 2013

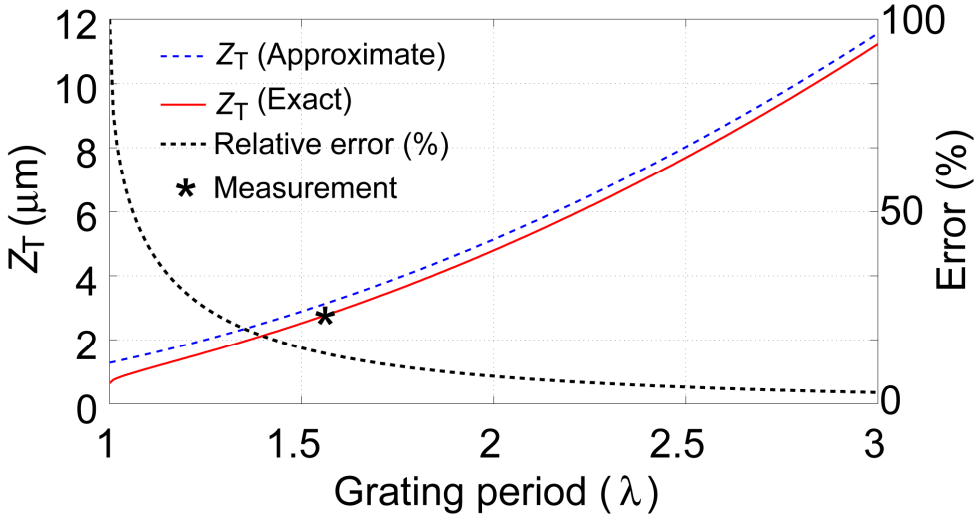

Fig. 3. Comparison of the exact and approximate Talbot lengths Z_T with respect to the grating period Λ. The difference becomes noticeable when the period Λ is below 5λ. The case of Λ = 1.56λ (= 1 μm) produces approximately 12% difference between two results. When Λ = λ, this relative error reaches up to 100%. The experimental result is in excellent agreement with the exact Talbot length.

4. Phase distributions: longitudinal-differential and propagation phase maps

In experiments, the longitudinal-differential interferometer naturally records the LD phase map as shown in Fig. 4(a). The experimental errors due to vibration and the laser source instability can now be corrected by using the *in situ* reference plane wave that is present in the region of x = 1 - 8 μm and which appears as a constant phase. By wrapping this constant phase of the reference plane wave with a modulo of 2π, a propagation phase map, which is the counterpart of the simulated absolute phase map, is obtained as shown in Fig. 4(b). The corresponding simulations are shown in Fig. 5. Note that the coordinates of the region of interest are shifted to match with intensity distributions. Therefore, the *in situ* reference appears now at x = 1 - 5 μm. The simulations are again in excellent agreement with experiments. In simulations, the absolute phase is the natural result that represents the propagation phase map as shown in Fig. 5(b). Subtracting the phase of the plane wave from the propagation map leads to the LD phase map in Fig. 5(a).

Especially in the low intensity region, e.g., in the geometrical shadow behind the 30-μm opaque region, the phase maps show much more information than the intensity maps. Now, the presence of the boundary diffraction wave is clearly observed on the left edge of the opaque region. The phase of the single diffraction order that does not superpose with other diffraction orders shows as a tilted planar wavefront on the right edge of the opaque region. In the region where the three diffraction orders superpose (x = 38 - 60 μm for experiment and x = 35 - 60 μm for simulation), phase Talbot images emerge from the grating surface. In this region, the super-resolution features like phase singularities are found in each self-image plane. Such phase dislocations occur where the destructive interference causes points in space with zero amplitude. Since only the self-images demonstrate such features [30], the position of the singularity can serve as an indication for the self-image planes. Therefore, a super-resolution distance measurement can be put in place when the phase field is considered for the applications exploiting the Talbot effect.

#179273 - $15.00 USD Received 5 Nov 2012; revised 21 Dec 2012; accepted 26 Dec 2012; published 11 Jan 2013

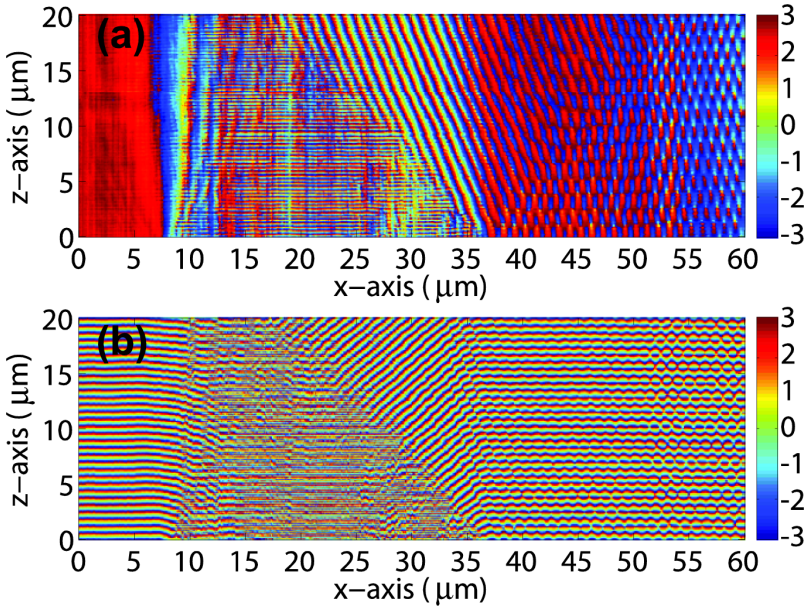

Fig. 4. The measured *x*-*z* phase distributions: (a) the longitudinal-differential phase map and (b) the propagation phase map. The reference plane wave passing the opening is shown in x = 1 - 8 µm of both maps in the referential plane at x = 0 µm. The propagation phase is obtained by adding the phase advance of a plane wave in free space to each distance that can be calculated analytically according to kz and unwrapping it with a modulo of 2π.

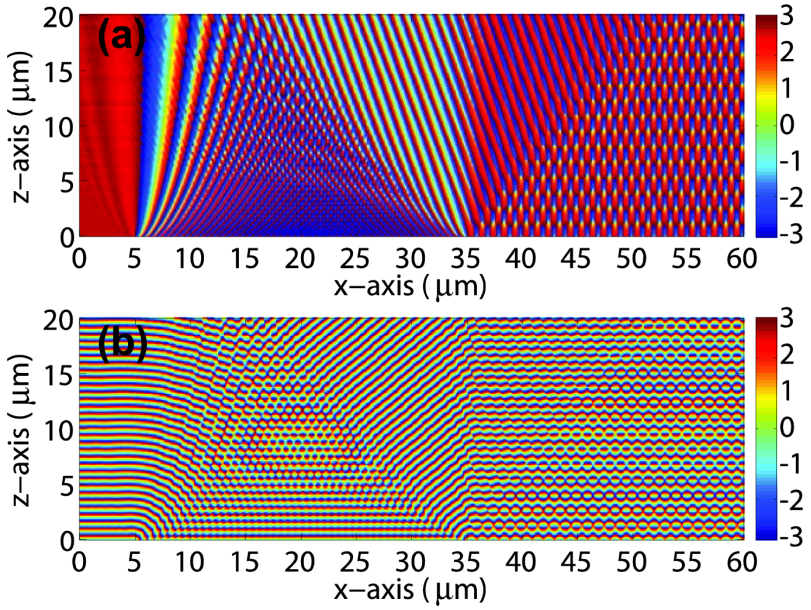

Fig. 5. The simulated *x*-*z* phase distributions: (a) the longitudinal-differential phase map and (b) the propagation phase map. The reference plane wave passing the opening is shown in x = 1 - 5 µm of both maps. The LD phase distribution is obtained by subtracting the phase of the plane wave from the propagation phase map in the referential plane at x = 0 µm.

#179273 - $15.00 USD Received 5 Nov 2012; revised 21 Dec 2012; accepted 26 Dec 2012; published 11 Jan 2013

5. Phase anomaly of the Talbot image

By definition, the classical Gouy phase of a focused, monochromatic field at an axial point is defined as the difference between the argument (or "phase") of the object field and that of a plane wave of the same frequency [77]. Here, we adopt this notion to discuss the phase anomaly of Talbot images. Therefore, the LD phase maps, which display the axial phase difference from the phase of the *in situ* reference plane wave, shown in Fig. 4(a) and 5(a) directly reveals the axial phase shift from the plane wave. Since Talbot images are periodic along the lateral direction, on-axis observation points are defined here as the points connecting the center of each Talbot image. Therefore, the axial profiles of the LD phase maps from the experiment [see Fig. 4(a)] and the simulation [see Fig. 5(a)] are extracted along the center of one Talbot image, i.e., close to x = 55 μm. After unwrapping they are plotted together in Fig. 6.

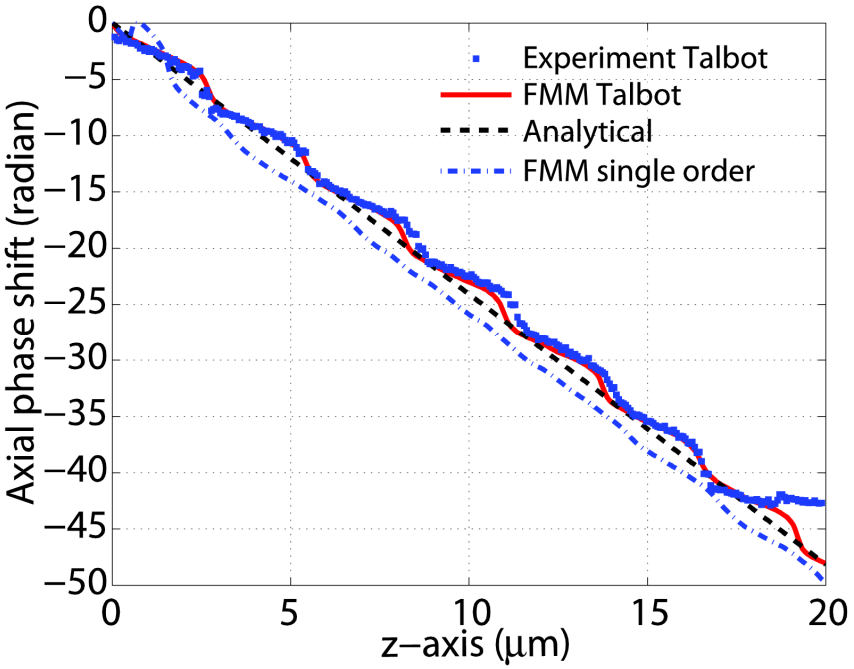

Fig. 6. The axial phase shifts along the center of Talbot images from the experiment (filled square) and simulation (red solid line). The analytical result using Eq. (3) is plotted in dark dashed line. For the single diffraction order, the simulation result is plotted in blue dot-dashed line denoted as FMM single order.

We observe a continuously growing phase shift along the z-axis. To better understand this phenomenon, an analytical equation is derived by using the tilted wave model [78]. In this model, the ± 1st orders are considered as propagating toward each other at a diffraction angle of 39.9° with respect to the surface normal. The superposition results in an interference that leads to Moiré-like fringes aligned along the axial direction. This Moiré interference fringe is superposed with the 0th diffraction order that is a plane wave propagating on-axis. Finally, the resulting interference between the Moiré-like fringe and the plane wave causes the axial periodicity, that is, the axial periodicity of the self-Talbot images. This suggests that the phase of the Talbot images can be written as the phase difference between the titled higher diffraction orders and the 0th order and is given as

$$\Delta\phi = z \cdot (\cos\theta - 1)k, \tag{3}$$

#179273 - $15.00 USD Received 5 Nov 2012; revised 21 Dec 2012; accepted 26 Dec 2012; published 11 Jan 2013

with θ being the diffraction (or tilt) angle and k being the wavenumber (= 2π/λ). In this case, the amount of the axial phase shift or phase anomaly $\Delta\phi$ does not has a finite and bound value, as in the case of a converging wave, but it is a growing function with respect to the propagation distance z. The phase anomaly calculated by Eq. (3) is also plotted in Fig. 6 and is compared to the experimental and numerical results. Overall, the analytical results show a very good agreement to the experiment and simulation. The axial phase of the single diffraction order, which is the −1st, has been plotted as well (see FMM single order). This will be discussed later with results of Fig. 7.

Apart from the main effect, which is the linearly growing phase anomaly defined by the analytical solution [see Eq. (3)], both the experimental and numerical results demonstrate periodic deviations from this linear slope. This clearly originates from the wavefront deformation and the irregular spacing within adjacent wavefronts. Talbot images are produced by three-waves-interference (the 0th and ± 1st orders) that causes the wavefront deformation appearing over one Talbot length [see Figs. 4(b) and 5(b) at x = 40 – 60 μm]. This results in an irregular wavefront spacing within one Talbot length, as shown in the extracted axial phase profile from Fig. 5(b) given in Fig. 7(a). Such irregular wavefront spacing is typically found in focused beams [63, 79, 80]. The irregularity causes a deviation of the phase from the linear slope as shown in Fig. 7(b), which is the phase anomaly occurring within one Talbot length (e.g., z = 0 - 2.8 μm). Therefore, the periodicity of this deviation in the Talbot image phase map is again equal to the Talbot length.

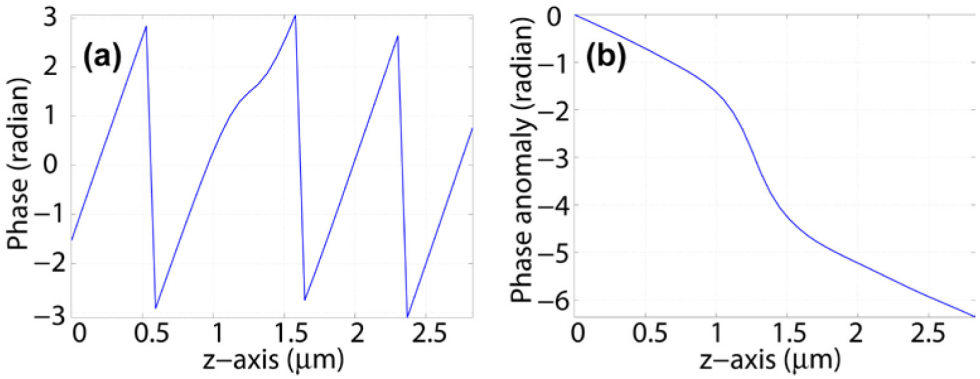

Fig. 7. Phase profiles within one Talbot length along the center of the Talbot image close to x = 55 μm: (a) the absolute phase from Fig. 5(b) and (b) the unwrapped LD phase from Fig. 5(a). The absolute phase shows the irregular wavefront spacing within one Talbot length. This irregularity leads to the phase anomaly slope deviating from the linear slope of the analytical solution Eq. (3). This repeatedly appears in Fig. 6 as a demonstration for the axial periodicity that represents the Talbot length.

The merit of our sample is the access to an isolated diffraction order that emerges from the left edge of the grating toward the opaque region. This single diffraction order, i.e., the −1st order, corresponds to a plane wave propagating obliquely at an angle of 39.9° with respect to the surface normal. In this case, the phase along the axial direction is defined by the longitudinal component of the wave number, $k_z = 2\pi/\lambda \cdot \cos\theta$, which represents exactly a tilted wave. Therefore, the axial phase difference of this isolated diffraction order from the plane wave propagating along the axial direction equals the result of Eq. (3). Now, the axial profile from the simulation from Fig. 5(a) is extracted at x = 34 μm for the −1st order. Since there is no wavefront deformation and irregular spacing, a periodic deviation from the linear slope is not found. The phase extracted from the simulation along this line is equally shown in Fig. 6 (see FMM single order) and shows clearly a linear slope at no specific periodic deviation. In this way, we can verify that the phase anomaly of the Talbot image is associated with the unified action of all the diffraction orders, for our case, the 0th and ± 1st orders, not the 0th order alone. The tilt angle θ (i.e., the diffraction angle of the higher orders) plays a key role to

#179273 - $15.00 USD Received 5 Nov 2012; revised 21 Dec 2012; accepted 26 Dec 2012; published 11 Jan 2013

define the growing slope. But the fine details are clearly dominated by the interference of multiple diffraction orders. For the Talbot images, the wavefront deformation and the irregular wavefront spacing causes periodic deviations from the linear slope that appear along the propagation distance. This periodicity verifies the Talbot length in another way. When the phase difference between higher (± 1st) orders and the lowest (0th) order equals 2π, constructive or destructive interference occurs. This suggests that the axial period of the Talbot images, which are the result of the constructive interference, equals the distance z where $\Delta\phi = 2\pi$. Therefore, by letting Eq. (3) = 2π another formulation of the Talbot length can be derived:

$$Z_T = \frac{\lambda}{1-\cos\theta}, \tag{4}$$

When applying the grating equation $\sin\theta = \lambda/\Lambda$, Eq. (1) leads to an identical formula as Eq. (4) that covers up to the non-paraxial case of the diffraction and interference problems.

6. Conclusions

We experimentally and theoretically investigated the phase anomaly in Talbot images close to 1D amplitude grating with a period only slightly larger than the illumination wavelength. Upon normal incidence, three propagating diffraction orders emerge, the 0th and ± 1st orders that have a diffraction angle of 39.9° in our specific geometry. With three interfering beams the minimal condition to generate Talbot images is fulfilled and self-images were found. The deflection angle of approximately 40° is well beyond the paraxial regime; consequently, the approximated equation for the Talbot length fails to agree with the experimental observations and rigorous simulations. The exact analytical equation derived by Lord Rayleigh is confirmed to be valid for such small period gratings and shows a perfect agreement with experimental and numerical results.

In order to provide the *in situ* reference plane wave as required for longitudinal-differential interferometry, particular grating structures were designed that sustain a wide opening far away from the edge of the grating. This opening permits the incidence plane wave to propagate with marginal perturbation so that the wavefront compares very well to that of the initial plane wave. The longitudinal-differential phase distributions, which are the natural outcomes of the experiments, directly demonstrate how much amount of axial phase shifts occur along the Talbot images. By wrapping this LD phase map with 2π modulo referencing the *in situ* plane wave, the propagation phase map could be obtained as well. Measurements were compared to simulations and showed an excellent agreement. Particular phase features like phase singularities were found in each self-image plane. There, destructive interference among the three propagating orders occurs at both sides of the bright Talbot images. It can be safely anticipated that these features can find application for super-resolution distance measurements, for instance.

The unwrapped axial phase profiles, which are extracted from the LD phase maps along the Talbot image center, allow the direct measurement of the phase anomaly in Talbot images. The main body of such self-images is the moiré-like interference fringe of two tilted waves, i.e., the ± 1st diffraction orders. This moiré fringe again interferes with the 0th order that corresponds to a plane wave propagating along the longitudinal direction with no deflection. Consequently, the phase difference between the tilted waves (i.e., the higher orders) and the normal plane wave (i.e., the 0th order) directly indicates the amount of the phase anomaly. By applying this concept, the analytical solution for the phase anomaly of the Talbot images has been derived and it matches well with experiments and simulations. Moreover, from this analytical solution of the phase anomaly, another formula for the Talbot length can be derived with respect to the tilt angle. The origin of the phase anomaly in the Talbot images is therefore the result of the phase difference between the higher diffraction orders and the 0th order caused by the tilt angle of the higher orders. Beyond increasing our understanding for the basic principles in such complicated beams, we may only speculate at

#179273 - $15.00 USD Received 5 Nov 2012; revised 21 Dec 2012; accepted 26 Dec 2012; published 11 Jan 2013

the moment that such research will find its way into applications such as a lensless image synthesis, into illumination systems and it may find use in various types of microscopes where structured illumination is at the heart to achieve images with super-resolving features.

Acknowledgment

The research leading to these results has received funding from the European Space Agency (ESA). C. Menzel and C. Rockstuhl would like to acknowledge funding from the German Federal Ministry of Education and Research (PhoNa) and the Thuringian State Government (MeMa). The authors are grateful to James R. Leger for careful reading and comments.

#179273 - $15.00 USD Received 5 Nov 2012; revised 21 Dec 2012; accepted 26 Dec 2012; published 11 Jan 2013